

## Flow pattern exchange in the Taylor-Couette system with a very small aspect ratio

Hiroyuki Furukawa,<sup>1,\*</sup> Takashi Watanabe,<sup>2,†</sup> Yorinobu Toya,<sup>3,‡</sup> and Ikuo Nakamura<sup>4,§</sup>

<sup>1</sup>Graduate School of Human Informatics, Nagoya University, Nagoya 464-8601, Japan

<sup>2</sup>Center for Information Media Studies, Nagoya University, Nagoya 464-8603, Japan

<sup>3</sup>Department of Mechanical Engineering, Nagano National College of Technology, Nagano 381-8550, Japan

<sup>4</sup>Department of Mechanical Engineering, Meijo University, Nagoya 468-8502, Japan

(Received 12 June 2001; revised manuscript received 20 November 2001; published 13 February 2002)

Numerical investigation is carried out on the flow pattern exchanges found in Taylor-Couette flows between two concentric rotating cylinders. The inner cylinder rotates while the outer cylinder and both end walls are stationary. The aspect ratio (column length/gap width) is small, and its range is from 0.5 to 1.6. Previous experimental results for this range of the aspect ratio showed that the steady flow patterns are classified into three groups: the normal two-cell mode, anomalous one-cell mode and twin-cell mode. All modes found by experiments are predicted in the present numerical calculation. Besides these three flow modes, an unsteady mode is predicted, which is time dependent and fully developed. The existence of the unsteady mode is also confirmed by our experiments. When the inner cylinder starts to rotate from rest, vortices at the corners of the inner cylinder and both end walls develop, and they induce the normal two-cell mode. The flow of the anomalous one-cell mode or twin-cell mode appears after an abrupt breakdown of symmetric two-cell mode flows. During the gradual deceleration of the inner cylinder, the transitions of flow modes occur. We observed mode transitions between the normal two-cell mode and anomalous one-cell mode and mode transitions from the twin-cell mode to the normal two-cell mode, anomalous one-cell mode, and unsteady mode. The critical loci where these mode transitions appear are determined. The numerical confirmation of the twin-cell mode is a different result obtained in the present study.

DOI: 10.1103/PhysRevE.65.036306

PACS number(s): 47.54.+r, 47.20.Ky, 47.32.-y

### I. INTRODUCTION

Taylor-Couette flow between two concentric rotating cylinders with finite axial length includes various patterns of laminar and turbulent flows, and its behavior has attracted great interest [1,2]. This flow is not only a classical stability phenomenon in fluid flows but also one of the most important problems of nonlinear sciences (for example, see [3,4]). For engineering applications, this flow is found in journal bearings, various fluid machinery, and chemical reactors. The unsteady development of flow pattern causes time-dependent variations of property values such as torque and rate of reaction, and it is, therefore, meaningful to investigate the transient behavior. The main parameters in Taylor-Couette flow are the Reynolds number  $Re$  based on the rotation speed of the inner cylinder, the aspect ratio  $\Gamma$  that is the ratio of the length of cylinders to the gap width between cylinders, and the radius ratio  $\eta$  of two cylinders. The flow at an infinite or moderate aspect ratio has provoked a great deal of controversy [5].

The seminal paper of Benjamin [6] followed by those of Benjamin and Mullin [7] and Mullin [8] unveiled a new dynamical aspect in the Taylor-Couette system with stationary end walls, and classified the modes of Taylor-Couette flow into primary and secondary modes. The primary mode appears when the Reynolds number is increased smoothly

from small values. The secondary mode occurs when the inner cylinder is abruptly accelerated above a certain value. Both primary and secondary modes have a normal mode and an anomalous mode. On each end wall, the flow of the normal mode has a normal cell that gives an inward flow in the region adjacent to the end wall. The flow of the anomalous mode has an anomalous cell that gives an outward flow near the end wall. Bolstad and Keller [9] showed that the stationary condition of the cylinder end walls may cause the anomalous mode. Nakamura *et al.* [10] and Toya *et al.* [11] observed the flows with stationary end walls and the flows with one stationary end wall and one free surface, respectively. They clarified bifurcation processes originating from the secondary modes, occasionally via another secondary mode, to the primary modes during the deceleration of the rotating inner cylinder. Alziary de Roquefort and Grillaud [12] and Sobolik *et al.* [13] confirmed that when the flow between rotating cylinders with finite length develops from rest, a secondary flow generates a vortex on the end wall, and Kuo and Ball [14] showed that as the vortex near the end wall develops, it induces other vortices in the area away from the end wall. Hill's numerical investigation [15] predicted four-cell and six-cell transitions found by Benjamin and Mullin [7], and concluded that reasonable agreement with the experimental results was obtained.

Some experimental studies on Taylor-Couette flow with an aspect ratio of about unity have been made. The experimental result of Benjamin and Mullin [7] revealed the existence of the single-cell mode, and presented the critical loci for the single-cell mode in the  $(\Gamma, Re)$  plane. Buzug *et al.* [16] found an oscillatory single-cell flow. Using flow visualization, Nakamura and Toya [17] confirmed that the flow of

\*Email address: hiroyuki@view.human.nagoya-u.ac.jp

†Email address: watanabe@view.human.nagoya-u.ac.jp

‡Email address: toya@me.nagano-nct.ac.jp

§Email address: inakamu@meijo-u.ac.jp

the anomalous mode had extra cells. They also found that the twin-cell flow appeared after the development of the extra cells. While there are a lot of experimental works on mode transitions at small aspect ratios, few numerical studies seem to have been done. Cliffe [18] used a finite element discretization for the steady Navier-Stokes equations and determined the critical loci for the single-cell mode in the  $(\Gamma, \text{Re})$  plane. Pfister *et al.* [19] used the steady equations and compared the numerical results with the experimental results in a very short annulus. The numerical investigations of Street and Hussaini [20] and Magère and Deville [21] confirmed the flow developing from the normal two-cell mode to the single-cell mode. However, more flow modes and mode exchanges are shown by the experimental work [17] than those found in these numerical studies.

Turing's paper [22] is a pioneering one about the pattern formation in the nonlinear dynamics, and it suggested the mathematical model of the chemical reaction-diffusion systems that may develop a pattern or structure due to an instability of the homogeneous equilibrium. After Turing, more and more studies have progressively appeared to analyze transient dynamics (for example, [23,24]). In the field of the Taylor-Couette system, however, in spite of complicated experimental results about transitional flow states [10,11], no detailed numerical study about this transient system is reported within our knowledge. The purpose of the present study is to predict the well developed flows and the flow-pattern transitions during the deceleration of the inner cylinder.

The aspect ratio is of order of unity ( $0.5 \leq \Gamma \leq 1.6$ ), and the inner cylinder rotates while the outer cylinder and both end walls are stationary. In the following, Sec. II describes the basic equations and numerical method used in the present study and Sec. III presents numerical results. Section IV gives a discussion on mode transitions and Sec. V gives conclusions.

## II. BASIC EQUATIONS AND NUMERICAL METHOD

The length of concentric two rotating cylinders is finite. The inner cylinder rotates, and the end walls and the outer cylinder are fixed. All physical parameters are made in dimensionless form by a reference length that is the gap width between two cylinders and a reference velocity, which is the maximum circumferential velocity of the inner cylinder attained during each run of a calculation. Dimensionless radii of the inner cylinder and the outer cylinder are  $r_i$  and  $r_o$ , respectively, and  $r_o - r_i = 1$ . The length of the cylinder is given by  $l$  and the aspect ratio  $\Gamma$  is defined by  $l/(r_o - r_i)$ . The Reynolds number based on the characteristic velocity is denoted by  $\text{Re}_0$ , and the Reynolds number based on an instantaneous rotation velocity of the inner cylinder is  $\text{Re}$ .

The governing equations are the unsteady axisymmetric Navier-Stokes equations and the equation of continuity expressed in the cylindrical coordinate system  $(r, \theta, z)$  that is suitable for the present calculation

$$r: \frac{\partial u}{\partial t} + u \frac{\partial u}{\partial r} + w \frac{\partial u}{\partial z} - \frac{v^2}{r} = -\frac{\partial p}{\partial r} + \frac{1}{\text{Re}_0} \left( \frac{\partial^2 u}{\partial r^2} + \frac{1}{r} \frac{\partial u}{\partial r} - \frac{u}{r^2} + \frac{\partial^2 u}{\partial z^2} \right), \quad (1)$$

$$\theta: \frac{\partial v}{\partial t} + u \frac{\partial v}{\partial r} + w \frac{\partial v}{\partial z} + \frac{uv}{r} = \frac{1}{\text{Re}_0} \left( \frac{\partial^2 v}{\partial r^2} + \frac{1}{r} \frac{\partial v}{\partial r} - \frac{v}{r^2} + \frac{\partial^2 v}{\partial z^2} \right), \quad (2)$$

$$z: \frac{\partial w}{\partial t} + u \frac{\partial w}{\partial r} + w \frac{\partial w}{\partial z} = -\frac{\partial p}{\partial z} + \frac{1}{\text{Re}_0} \left( \frac{\partial^2 w}{\partial r^2} + \frac{1}{r} \frac{\partial w}{\partial r} + \frac{\partial^2 w}{\partial z^2} \right), \quad (3)$$

$$\frac{1}{r} \frac{\partial(ru)}{\partial r} + \frac{\partial w}{\partial z} = 0, \quad (4)$$

where  $t$  is time,  $(u, v, w)$  is the velocity components in the directions of  $(r, \theta, z)$  and  $p$  is the pressure.

The basic solution procedure is the marker and cell (MAC) method. The Poisson equation for pressure is as follows:

$$\begin{aligned} \frac{\partial^2 p}{\partial r^2} + \frac{1}{r} \frac{\partial p}{\partial r} + \frac{\partial^2 p}{\partial z^2} = & - \left( \frac{\partial u}{\partial r} \frac{\partial u}{\partial r} + \frac{\partial w}{\partial z} \frac{\partial w}{\partial z} + 2 \frac{\partial u}{\partial z} \frac{\partial w}{\partial r} \right. \\ & \left. + 2 \frac{1}{r} \frac{\partial v}{\partial z} - 2 \frac{v}{r} \frac{\partial v}{\partial r} + \frac{u^2}{r^2} \right) \\ & - \frac{\partial D}{\partial t} - u \frac{\partial D}{\partial r} - w \frac{\partial D}{\partial z}, \end{aligned} \quad (5)$$

where  $D$  is divergence of the velocity vector. A hybrid method of successive over-relaxation method (SOR) and conjugate gradient squared method with incomplete lower and upper triangular matrices decomposition preconditioning (ILUCGS) is used to solve the Poisson equation. The time integration is the Euler explicit method, and the spatial differentiation is the quadratic upstream interpolation for convective kinematics (QUICK) method for convection terms and the second-order central difference method for other terms [25].

The boundary conditions for the velocity components on the cylinder walls and both end walls are the no-slip conditions. The pressure boundary conditions are the Neumann conditions that are obtained from the pressure terms of momentum equations. The initial values of all velocity components are zero in the entire domain. At  $t=0$ , the Reynolds number abruptly changes from zero to  $\text{Re}_0$ .

The staggered grid is adopted and the grid interval is uniform in each direction. The number of grid points in the radial direction is 80, and the number of grid points in the axial direction is determined by the proportionality to the cylinder length with 80 points for the aspect ratio of unity.

Even though the grids were refined by halving the spacing in each direction, the difference of the numerical results is well less than 1%. This ensures that the number of grid points used in the present calculation is large enough not to exert observable influence on results.

When the time variation of relative torque on cylinders remains less than  $10^{-4}$ , a steady state of time-developing flow is judged to be attained. For the calculations of the decelerating flows, the Reynolds number begins to decrease when a fully steady state is established at  $t=t_1$ , and the linear decrease continues from  $t=t_1$  to  $t_1+t_2$ . After the deceleration, the Reynolds number is kept constant again.

The Stokes' stream function  $\psi$  for the flow visualization is given by

$$u = -\frac{1}{r} \frac{\partial \psi}{\partial z}, \quad w = \frac{1}{r} \frac{\partial \psi}{\partial r}. \quad (6)$$

The results of the present calculation are compared with experimental results obtained by Nakamura and Toya [17]. Their experimental apparatus had an inner cylinder with a radius of 20 mm and an outer cylinder with a radius of 30 mm, and the radius ratio  $\eta$  is 0.667. The dimensionless times  $t_1$  and  $t_2$  correspond to 50 seconds in the dimensional form when they are evaluated with the physical dimensions of cylinders and the kinematic viscosity ( $6 \times 10^{-6}$  m<sup>2</sup>/s) of aqueous solution of glycerol used in their experiment. The range of the Reynolds numbers is from 100 to 1500. In the following, for the purpose of better understanding, the  $z$  coordinate is normalized not by the characteristic length but by the axial length of the working fluid  $l$ .

### III. RESULTS

#### A. Steady mode in fully developed flow

In this section, steady-state flows established after a sudden start of the inner cylinder are presented. Figure 1 shows three steady modes: normal two-cell mode, anomalous one-cell mode, and twin-cell mode. It displays the contours of the stream function  $\psi$  in the meridional section, and the rotating inner cylinder is on the left and the stationary outer cylinder is on the right. The end wall would be refereed as an upper or lower wall, if necessary. The contours of the stream function are accompanied by plus symbols  $\oplus$ , which indicate that the rotating direction of vortices is clockwise, and minus symbols  $\ominus$ , which indicate that the rotating direction is counterclockwise.

When the Reynolds number is small, stable flows of the normal two-cell mode are formed. The normal two-cell mode flow in Fig. 1 gives inward flows near the end walls, and the flow is outward between cells. The terminal points of the boundary between two cells are on the inner and outer cylinder walls. A symmetric flow pattern and an asymmetric flow pattern appear as shown in Fig. 1(a) and Fig. 1(b), respectively. The asymmetric pattern is established via a pitchfork bifurcation from the symmetric flow [19]. Even in the asymmetric flow, each cell extends on the whole region of one end wall, and it does not reach both end walls.

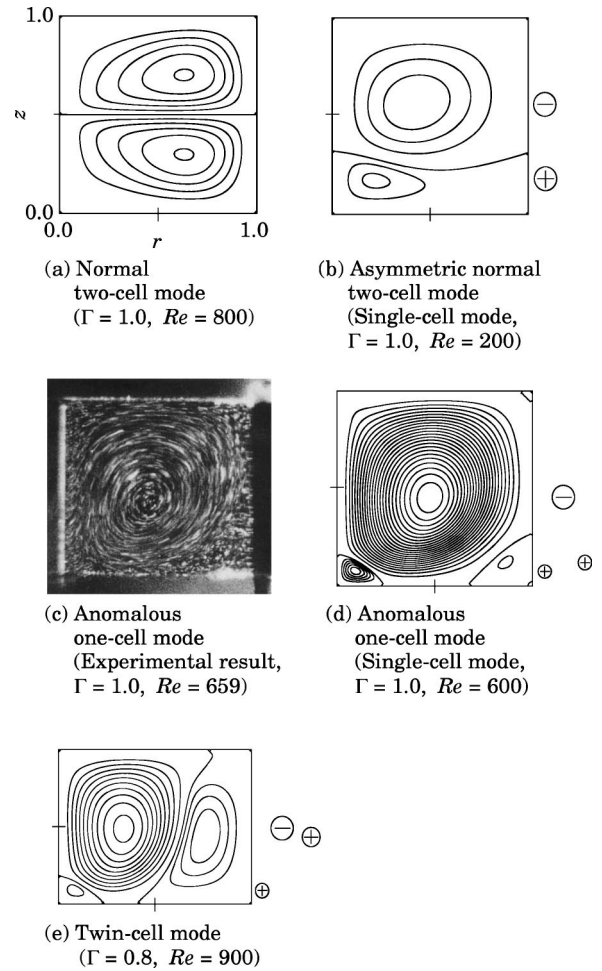


FIG. 1. Contours of the stream function in the flows with normal two-cell mode, anomalous one-cell and twin-cell modes. Symbols  $\oplus$  and  $\ominus$  indicate the clockwise and counterclockwise rotating directions, respectively. The intervals of the stream function are as follows. (a) 0.01. (b) 0.014 for main vortex and 0.0047 for small vortex at inner lower corner. (d) 0.003 for main vortex and 0.0006 for two small vortices at lower corners. (e) 0.005 for left large vortex at inner upper corner and 0.0023 for other vortices.

Figure 1(d) shows an example of the anomalous one-cell mode. The main cell is anomalous, and it rotates in the counterclockwise direction. Two extra cells rotating in the clockwise direction accompany the anomalous cell: one is at the inner lower corner and the other is at the outer lower corner. The terminal points of the boundaries between the anomalous cell and extra cells are on the inner or outer cylinder wall and the end wall to which the extra cells are attached. The calculated flow pattern agrees with the experimental result shown in Fig. 1(c). Cliffe [18] obtained three distinct flow patterns by calculations, which are “stable two-cell mode,” “unstable asymmetric flow,” and “single-cell mode.” Both the asymmetric normal two-cell mode shown in Fig. 1(b) and the anomalous one-cell mode shown in Fig. 1(d) are what are called “single-cell mode” by Cliffe. The asymmetric two-cell mode has no extra cell and the anomalous one-cell mode has extra cells at the corners of the annulus, and they need to be classified as different mode from

each other. Therefore, the present paper distinguishes the asymmetric normal two-cell mode from the anomalous one-cell mode.

When the aspect ratio is from 0.6 to 0.9 and the Reynolds number is from 1000 to 1500, the twin-cell mode is established [Fig. 1(e)]. Two large cells and one small extra cell appear. The small extra cell is located at the inner lower corner. One terminal point of the boundary between two large cells is on the end wall opposite to the wall to which the extra cell is attached.

### B. Formation process of the steady mode

At the beginning of the mode formation process of the normal two-cell mode, two vortices appear at the inner upper and inner lower corners. After they touch with each other at the midplane in the axial direction, they grow in the radial direction. Finally, the flow field becomes a stable normal two-cell mode [Fig. 1(a)].

In the mode formation process of the anomalous one-cell mode, two large vortices grow, and the normal two-cell mode, which is mentioned above, is established as an intermediate state. Then, one vortex collapses the other vortex and reaches both end walls. The collapsed vortex is divided into two extra cells at the inner and outer cylinder sides, and the anomalous one-cell mode appears [Fig. 1(d)].

The mode formation process of the twin-cell mode is as follows. After the normal two-cell mode flow is formed, one vortex becomes dominant. The dominant vortex divides the other vortex into two small vortices. The divided small vortex at the inner cylinder side remains as an extra cell at the corner between the inner cylinder wall and the end wall. The other small vortex at the outer cylinder side does not decay but develops gradually. The developing vortex touches with the upper and lower end walls, and it becomes as large as the dominant vortex. The dominant vortex is in the inner half of the flow region and the developed vortex is in the outer half region [Fig. 1(e)].

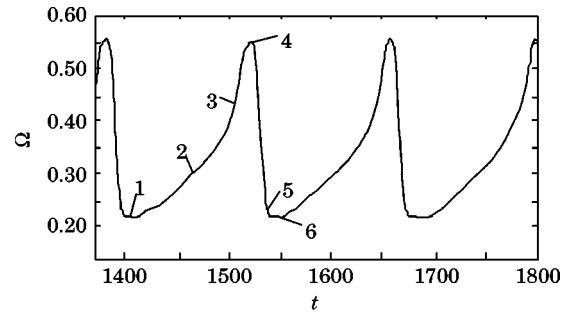
### C. Unsteady mode in fully developed flow

An unsteady and fully developed flow mode appears other than the normal two-cell mode, anomalous one-cell mode, and twin-cell mode mentioned in Sec. III A. Here after, this time-dependent mode is called an unsteady mode. In order to distinguish various global flow patterns, we need to introduce some measures. The spatially averaged enstrophy and the kinetic energy have clear physical meanings, and they are deserved to be the suitable measures of the flow field. We present the mean enstrophy  $\Omega$  that is given by

$$\Omega = \frac{1}{A} \int_S \frac{1}{2} \left( \frac{\partial u}{\partial z} - \frac{\partial w}{\partial r} \right)^2 dr dz, \quad (7)$$

where  $S$  is an integral domain and  $A$  is the area of a meridional section.

Figure 2 shows the profiles of the unsteady mode flow. The aspect ratio is 0.5 and the Reynolds number is 1500. The time variation in the mean enstrophy is shown in Fig. 2(a). The numbers from 1 to 6 denote the time points that are



(a) Time variation in the mean enstrophy

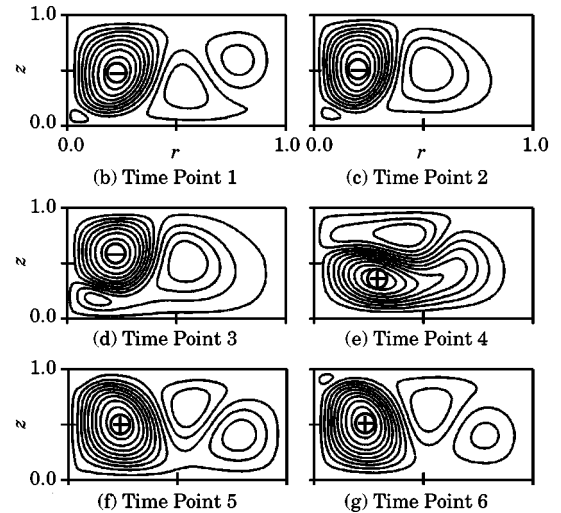


FIG. 2. Unsteady motion. (a) Time variation in the mean enstrophy of the unsteady mode flow. (b)–(g) Variations in the streamlines of the unsteady mode flow. Time points are shown in (a). The main vortex in each figure is accompanied by the symbol  $\oplus$  that indicates the clockwise rotating direction or the symbol  $\ominus$  which indicates the counterclockwise direction. The aspect ratio is 0.5 and the Reynolds number is 1500.

referred to in Figs. 2(b)–2(g). The time variation in the mean enstrophy is not smooth and the value decreases suddenly from the time point 4 to 5. The mean kinetic energy in the meridional section has variation similar to that of the mean enstrophy. Figures 2(b)–2(g) include the contours of the stream function  $\psi$  at each time point. At time point 1 [Fig. 2(b)], the flow has four vortices and a small vortex appears at the inner lower corner. The mean enstrophy is minimum at this time point. As the mean enstrophy increases, the vortex closest to the outer cylinder decays and three vortices remain [Fig. 2(c)]. When the mean enstrophy increases further, the inner small vortex and outer vortex merge [Fig. 2(d)]. The enstrophy is maximum at the time point 4 [Fig. 2(e)] at which two large vortices appear. Then each vortex is split by the other [Fig. 2(f)] and four vortices emerge [Fig. 2(g)]. The flow at the time point 6 is almost mirror symmetric with the flow at the time point 1. After the time point 6, the flow field traces back from the time point 5, via the time points 4, 3, and 2, to the time point 1. From this, two periods in the variation of the mean enstrophy in Fig. 2(a) correspond to

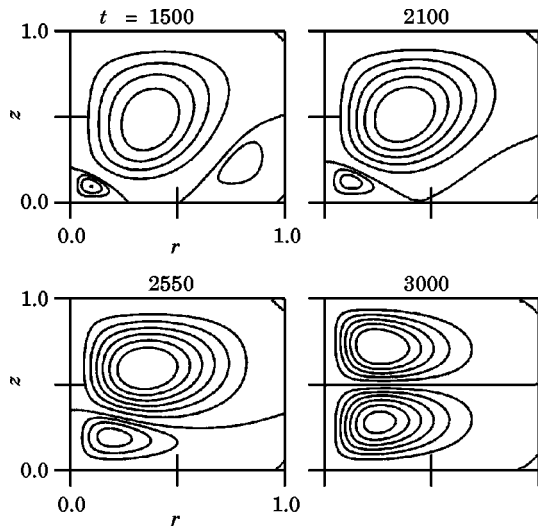


FIG. 3. Development of the flow field from the anomalous one-cell mode to the normal two-cell mode. The aspect ratio is 0.8 and the Reynolds number is decreased from 500 at  $t = 1500$  to 100 at  $t = 3000$ .

one period of the unsteady motion shown in Figs. 2(b)–2(g). When the flow traces back from the time point 6 to 1, the change in the flow pattern is slow from the time point 6 to 4 and it is rapid from the time point 4 to 1. The mean enstrophy varies at uniform period even after a long time.

#### D. Mode transition

When fully developed flows at specific Reynolds numbers are decelerated, transitions to other mode flows appear [10]. The mode transitions among the normal two-cell mode, anomalous one-cell mode, and twin-cell mode have been observed during or after the gradual decrease in the Reynolds number.

Figure 3 shows the time variation of the stream lines during the mode transition from the anomalous one-cell mode to the normal two-cell mode. The aspect ratio is 0.8 and the Reynolds number is linearly decreased from 500 at  $t = 1500$  to 100 at  $t = 3000$ . Though a similar transition has been observed during the reduction of the Reynolds number from 350 to 340, Fig. 3 is shown for the better understanding of the transition. At  $t = 1500$ , the flow field is the anomalous one-cell mode that is stable at  $Re = 500$ . An anomalous cell accompanies extra cells at the inner and outer cylinder sides. As the rotation speed decreases, the extra cells approach each other and merge into one new normal cell, and the normal two-cell mode appears ( $t = 2550$ ). The mode transition from the normal two-cell mode to the anomalous one-cell mode was also observed when the Reynolds number was decelerated. The flow pattern traced back the mode formation process shown in Fig. 3.

The boundaries between the normal two-cell mode and the anomalous one-cell mode in the  $(\Gamma, Re)$  plane are shown in Fig. 4. They are delimited at the left and right hands of the range of  $\Gamma$  where the mode bifurcations between these two modes do not appear. In the regions denoted by A and C, the normal two-cell mode appears, and the region where the

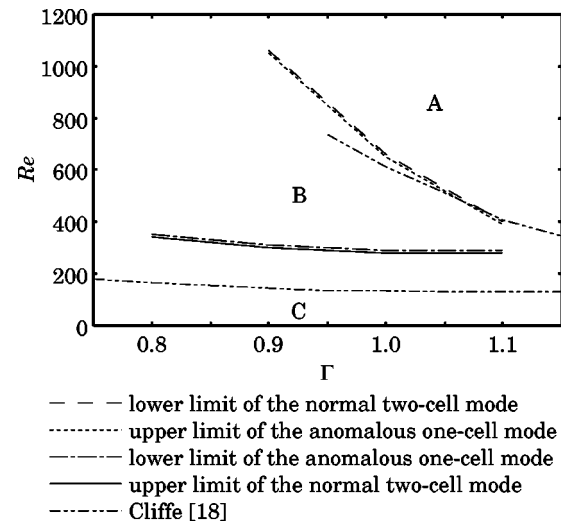


FIG. 4. Transitions from the anomalous one-cell mode to the normal one-cell mode and transitions from the normal two-cell mode to the anomalous one-cell mode. A and C, regions where the normal two-cell mode appears. B, region where the anomalous one-cell mode appears.

anomalous one-cell mode exists is indicated by (B). At a constant aspect ratio, the flow changes from the normal two-cell mode to the anomalous one-cell mode when the Reynolds number on or above the lower limit of the normal two-cell mode is reduced to the Reynolds number on or below the upper limit of the anomalous one-cell mode. The difference of the Reynolds number between the upper and the lower limits are 10.0 and the deceleration is slowed. Similarly, the change from the anomalous one-cell mode to the normal two-cell mode occurs when the Reynolds number on or above the lower limit of the anomalous one-cell mode is decreased to the Reynolds number on or below the upper limit of the normal two-cell mode. Cliffe's result [18] obtained by using the steady equations is also given in Fig. 4. Though the radius ratio of the present study (0.667) is larger than that used by Cliffe (0.615), the qualitative agreement demonstrates the validity of the present study. Cliffe *et al.* [26] showed that the lower critical Reynolds numbers at which the anomalous mode loses its stability becomes larger as the radius ratio increases. The result obtained in the present study is not inconsistent with Cliffe's results.

Figure 5 shows the mode transition from the twin-cell mode to the anomalous one-cell mode at the aspect ratio 0.8 and the reduction of the Reynolds number from 1000 to 600. At  $t = 3000$ , the flow mode is the twin-cell mode with an extra cell around the inner lower corner. As the rotation speed decreases, the separation point on the upper end wall gradually shifts outward and moves onto the outer cylinder. Then the flow becomes the anomalous one-cell mode ( $t = 4800$ ).

The mode transition from the twin-cell mode to the normal two-cell mode, anomalous one-cell mode and unsteady mode were observed. Figure 6 denotes the bifurcation loci separating the twin-cell mode from other modes in the  $(\Gamma, Re)$  plane. The bifurcation loci end at the left- and right-hand sides of the figure where the twin-cell mode does not appear.

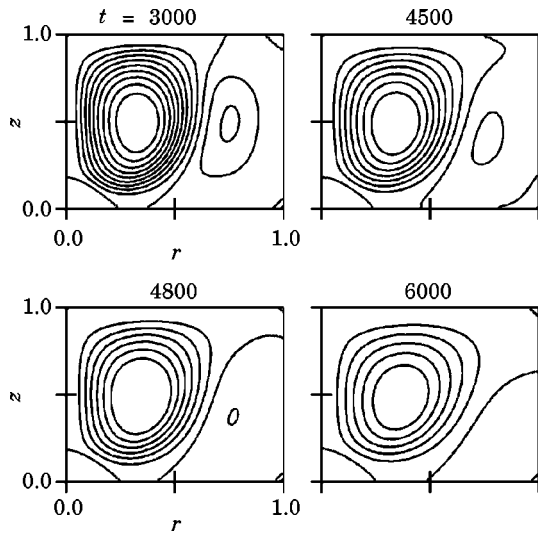


FIG. 5. Development of the flow field from the twin-cell mode to the anomalous one-cell mode. The aspect ratio is 0.8 and the Reynolds number is decreased from 1000 at  $t=3000$  to 600 at  $t=6000$ .

The flow mode is the twin-cell mode at the Reynolds number above the line A-B. At the Reynolds number below the lines C-D, D-E and E-F, the unsteady mode, the normal two-cell mode and the anomalous one-cell mode appear, respectively. When the aspect ratio is constant and the Reynolds number changes from the value on or above the line A-B to the value on or below the line C-D-E-F, the mode transitions from the twin-cell mode to the other mode occur. The critical loci have their minima at  $\Gamma=0.74$  where the flow mode changes from the twin-cell mode to the normal two-cell mode during the reduction of the Reynolds number from 680 to 670.

IV. DISCUSSION

The twin-cell mode has been obtained only by the experiment [17], and the numerical confirmation of the twin-cell mode is a different evidence obtained in the present study. The bifurcation loci from the twin-cell mode are also presented in this paper.

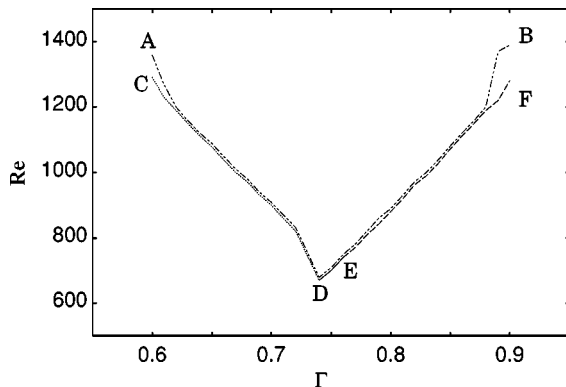


FIG. 6. Transition from the twin-cell mode. A-B : lower limit of the twin-cell mode. C-D: upper limit of the unsteady mode. D-E: upper limit of the normal two-cell mode. E-F : upper limit of the anomalous one-cell mode.

When the Reynolds number exceeds a certain value, Taylor-Couette flow forms time-dependent azimuthal waves. For a relatively small aspect ratio at which the two-cell or four-cell mode appears, Mullin and Benjamin [27] presented the critical Reynolds number for the onset of the wavy motion. On the other hand, Pfister *et al.* [19], Eagles [28], and Gerdts *et al.* [29] reported an unstable axisymmetric oscillation of the two-cell flow. Using the experimental apparatus mentioned in Toya *et al.* work [11], we have investigated flows with the small aspect ratio 0.5, and found the unsteady motion. Though the sizes and positions of vortices change, the flow is not wavy. The unsteady flow motion found by this experiment has the same order of the period as the one predicted by the numerical result in Fig. 2(a). Pfister *et al.* [19] obtained the nondimensionalized frequency for the axisymmetric oscillation. The nondimensional frequency of the unsteady mode shown in Fig. 2(a) is 0.047 and the unsteady mode described in Sec. III C corresponds to the axisymmetric oscillation revealed by Pfister *et al.* While Pfister *et al.* called the oscillation of the flow as “new two-cell flow,” Figs. 2(b) and 2(g) show that not only two vortices but more vortices appear during the unsteady motion.

The anomalous one-cell mode, twin-cell mode, and unsteady mode have flow patterns asymmetric with respect to the midplane in the axial direction. Pfister *et al.* [19] described that imperfections of the apparatus would disconnect the supercritical bifurcations and the single-cell mode has a duality of the flow states in which a large main vortex and a small weak vortex appear near the top or bottom plate, respectively. Both states were observed in the experiment although one state was obtained only by a tricky way such as a sudden start of the inner cylinder. Besides the imperfections of the apparatus, the candidates of the factors that select a solution branch in the bifurcation diagram may be a thermal disturbance and an incomplete steadiness of an initial state. In the calculation, one of the counterparts of the imperfections is the residual of the numerical scheme. In the present calculation, the reversed sequence of pressure variables in the Poisson equation has resulted in mirror symmetric images of flow patterns with respect to the midplane.

V. CONCLUSIONS

In order to clarify some aspects of the transitional phase in the nonlinear system, the fully developed Taylor-Couette flow between two concentric rotating cylinders with very short lengths has been investigated by the time-dependent numerical method. The aspect ratio is of the order of unity, and the inner cylinder rotates while the outer cylinder and end walls of the cylinders remain stationary. Developing processes of flow modes are predicted. Mode transitions during the gradual deceleration of the rotation speed of the inner cylinder are clarified.

The existence of the normal two-cell mode, anomalous one-cell mode, and twin-cell mode is confirmed. In the mode formation processes of the anomalous one-cell mode and twin-cell mode, almost symmetric flow patterns are formed at first, and then the symmetries break down.

An unsteady mode of the fully developed flow, which is not wavy Taylor-Couette flow, is obtained. The periods of the unsteady flow in the experiment and the calculation are of the same order. In this mode, each vortex splits the other vortex at high Reynolds numbers. One period of the dynamic movement of flow fields corresponds to two periods of the time variation of the mean enstrophy.

Transitions between the normal two-cell mode and anomalous one-cell mode and transitions from the twin-cell mode to the normal two-cell mode, anomalous one-cell mode and unsteady mode are predicted, and the bifurcation loci are obtained. In the transition between the normal two-cell mode and anomalous one-cell mode, the growth or decay of the extra cells plays a main role.

- 
- [1] P. Chossat and G. Iooss, *The Couette-Taylor Problem* (Springer-Verlag, Berlin, 1994).
- [2] C.D. Andereck and F. Hayot, *Ordered and Turbulent Patterns in Taylor-Couette Flow* (Plenum Press, New York, 1992).
- [3] H.L. Swinney and J.P. Gollub, *Hydrodynamic Instabilities and the Transition to Turbulence* (Springer-Verlag, Berlin, 1981).
- [4] G.S. Lewis and H.L. Swinney, Phys. Rev. E **59**, 5457 (1999).
- [5] E.L. Koschmieder, *Benard Cells and Taylor Vortices* (Cambridge University Press, Cambridge, 1993).
- [6] T.B. Benjamin, Proc. R. Soc. London, Ser. A **359**, 27 (1979).
- [7] T.B. Benjamin and T. Mullin, Proc. R. Soc. London, Ser. A **377**, 221 (1981).
- [8] T. Mullin, J. Fluid Mech. **121**, 207 (1982).
- [9] J.H. Bolstad and H.B. Keller, J. Comput. Phys. **69**, 230 (1987).
- [10] I. Nakamura, Y. Toya, S. Yamashita, and Y. Ueki, JSME Int. J., Ser. II **33**, 685 (1990).
- [11] Y. Toya, I. Nakamura, S. Yamashita, and Y. Ueki, Acta Mech. **102**, 137 (1994).
- [12] T. Alziary de Roquefort and G. Grillaud, Comput. Fluids **6**, 259 (1978).
- [13] V. Sobolik, B. Izrar, F. Lusseyran, and S. Skali, Int. J. Heat Mass Transf. **43**, 4381 (2000).
- [14] D.C. Kuo and K.S. Ball, Phys. Fluids **9**, 2872 (1997).
- [15] N.A. Hill, Comput. Fluids **16**, 445 (1988).
- [16] Th. Buzug, J. von Stamm, and G. Pfister, Physica A **191**, 559 (1992).
- [17] I. Nakamura and Y. Toya, Acta Mech. **117**, 33 (1996).
- [18] K.A. Cliffe, J. Fluid Mech. **135**, 219 (1983).
- [19] G. Pfister, H. Schmidt, K.A. Cliffe, and T. Mullin, J. Fluid Mech. **191**, 1 (1988).
- [20] C.L. Streett and M.Y. Hussaini, *Finite Length Taylor Couette Flow, Stability of Time Dependent and Spatially Varying Flows* (Springer-Verlag, Berlin, 1988), pp. 663–675.
- [21] E. Magère and M.O. Deville, Appl. Numer. Math. **33**, 241 (2000).
- [22] A.M. Turing, Philos. Trans. R. Soc. London, Ser. B **237**, 37 (1952).
- [23] Y. Kuramoto, *Chemical Oscillations, Waves, and Turbulence* (Springer-Verlag, Berlin, 1984).
- [24] Z. Neufeld, C. López, E. Hernández-García, and T. Tél, Phys. Rev. E **61**, 3857 (2000).
- [25] D.A. Anderson, J.C. Tannehill, and R.H. Pletcher, *Computational Fluid Mechanics and Heat Transfer* (Hemisphere Publications, New York, 1984).
- [26] K.A. Cliffe, J.J. Kobine, and T. Mullin, Proc. R. Soc. London, Ser. A **439**, 341 (1992).
- [27] T. Mullin and T.B. Benjamin, Nature (London) **288**, 567 (1980).
- [28] P.M. Eagles, Phys. Fluids **10–12**, 3080 (1998).
- [29] U. Gerds, J. von Stamm, Th. Buzug, and G. Pfister, Phys. Rev. E **49**, 4019 (1994).